Application of Discrete Wavelet Transform to the Analysis of a Submarine Cable Trip

By: Dean Sorensen, Song Ji, Dan Benoit – National Grid USA (National Grid)

Introduction

Correct and rapid fault clearing as well as minimizing power outage durations are important utility company concerns. Protections work to isolate faults and quickly to minimize system impacts while analysis should facilitate timely restoration. This paper examines tripping of an undersea cable by a numerical line differential (87L) relay. While conventional DFR data analysis was helpful for determining where the fault was not, it was unable to determine where the fault was, including which end of the zone was faulted. The DFR record also did not explain well the nature of the fault. After the fact, the use of discrete wavelet transform methods was explored in an effort to improve our ability to determine the nature of the fault and hopefully correlate its location with other forensic details.

The cable in question is one of two undersea cables connecting a popular vacation island off the coast of Massachusetts to the mainland transmission grid at two different locations. Each undersea cable is about 30 miles in length including some underground cable on the mainland side. Each undersea cable terminates at a 40MVA transformer in a double-ended straight bus station on the island. Also on the island, there exists a 15MVA combustion turbine generator (CTG) serving as a backup supply for the loss of a single undersea cable and a 7.5MVA battery energy storage system (BESS) to facilitate a bumpless load transfer to and from the CTG. *Figure 1* illustrates these details.

System Overview

There are two interconnection points that are 4 towns apart (M-Way and L-Ave subs) on the mainland 115kV transmission grid. The mainland grid belongs to a neighboring transmission owner (TO). At both interconnection stations voltage steps down from 115kV to a 46kV bus on which each undersea cable terminates. Both cables are roughly 30 miles in length and each cable produces roughly 8 MVAR of capacitive charging power. Consequently, there exists at each mainland station two stages of 4 MVAR shunt reactors that both consume reactive power and control voltage at the mainland end of the cables. Refer to *Figure 1* for details.

Both undersea cables terminate on the North side of the island at C-Street sub, which is a double-ended straight-bus station with a normally open tie breaker. On the South side of the island the B-Rd sub is normally supplied by C-Street T1 transformer. There is an alternate feed from C-Street sub T2 which is omitted because it was not relevant to this study. At B-Rd station there is the CTG as well as the BESS.

Figure 1: Area 1-Line Diagram

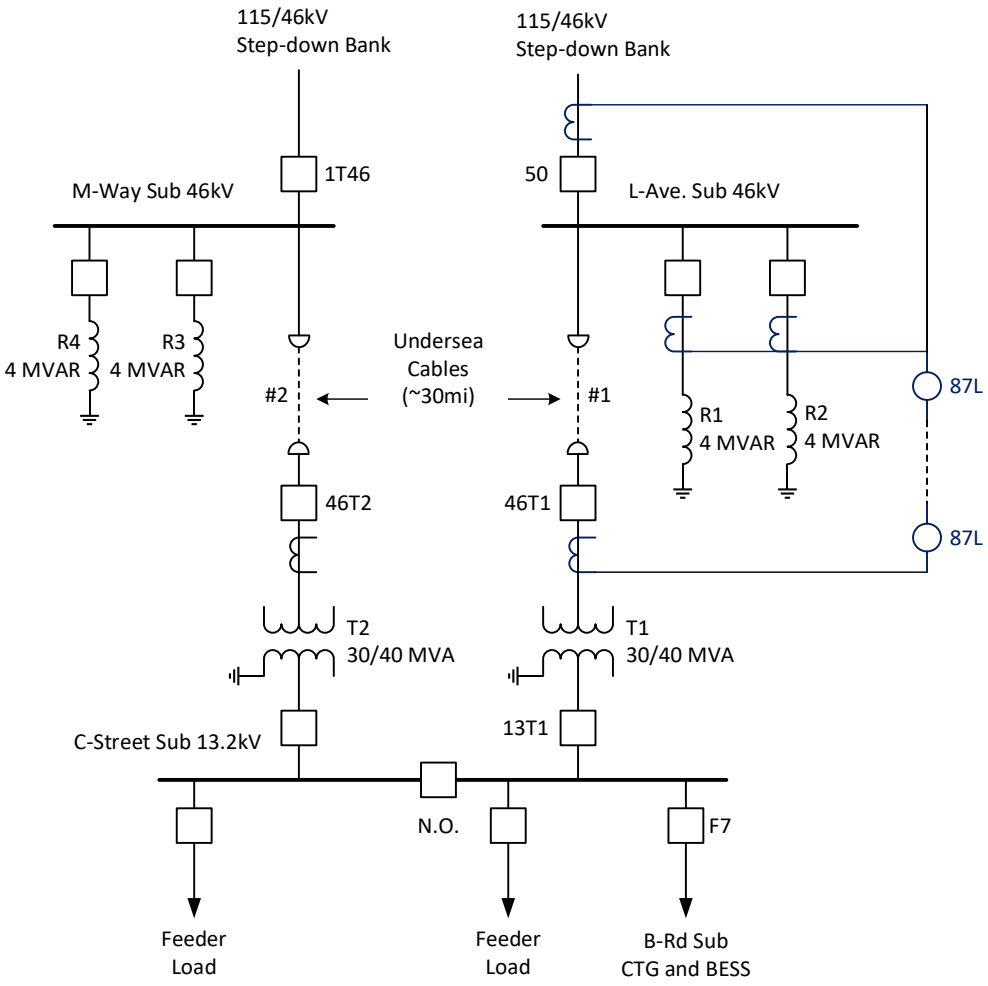

Incident Summary

On April 30, 2024, the #1 undersea cable tripped via 1990's vintage charge comparison type numerical line differential (87L) relays. This was a fair-weather day with no precipitation and 0-12mph winds. No unusual events or debris were reported in and around the areas of the L-Ave sub on the mainland nor the C-St sub on the island. While the 87L relay indicated the fault type with phase AB targets, no oscillograph record was generated. Neither was any distance-to-fault (DTF) data generated. Mainland side (L-Ave) backup 21/21N relays did not operate nor generate an event record. No other protections operated. The only fault record available was one captured by a temporary DFR that was installed at L-Ave sub to monitor the cable.

Conventional Investigation and Analysis of the Event

With the temporary DFR at L-Ave providing the only fault record and few physical clues, there was a bare minimum of data available for analysis. Being just a few weeks before the Memorial Day kickoff of the summer vacation season, management had serious concerns over the condition of the undersea cable and its ability to serve island load over the summer.

So where was the fault? In the undersea cable? In the approximately 3 miles of underground cable between L-Ave sub and the beach before transitioning to undersea cable? Somewhere in the L-Ave overhead bus or the lightning arrestors protecting the cable? Somewhere in the C-St 46kV GIS breaker switchgear? An analysis of the sole DFR record did provide some clues. The record indicated the fault configuration to be phase-to-phase (AB) with no ground involvement. The fault self-cleared in about 10ms (0.6 cycles) after which the ABC load currents returned to previous pre-fault magnitudes with normal phase spacing. The L-Ave 3-cycle breaker interrupted the load current about 44ms (2.64 cycles) after the fault self-cleared. The pre and post fault current magnitude was about 100A with the RMS value of the first half-cycle of fault current being about 424A. Refer to *Figure 3* for DFR record details.

Figure 2: Cross-section of Similar 72kV Undersea Power Cable

An analysis of the DFR record could not positively determine where the fault was. However, it could reliably indicate where the fault was not. Referring to the physical cable construction shown in *Figure 2*, it becomes clear that the fault could not have been in the underground or undersea portions of the cable differential zone. There is simply no way to establish a phase-to-phase fault without involving the two grounded shields surrounding the two faulted phases. The DFR record clearing indicated that this fault included no ground involvement. Beyond that, the fault record provided no clear indication as to the fault's location. The fault having self-cleared strongly suggested that the fault wasn't permanent.

That fact plus the relatively low fault magnitude suggested partial discharge (PD) activity was the likely cause of this event.

Figure 3: L-Ave Sub Portable DFR Record

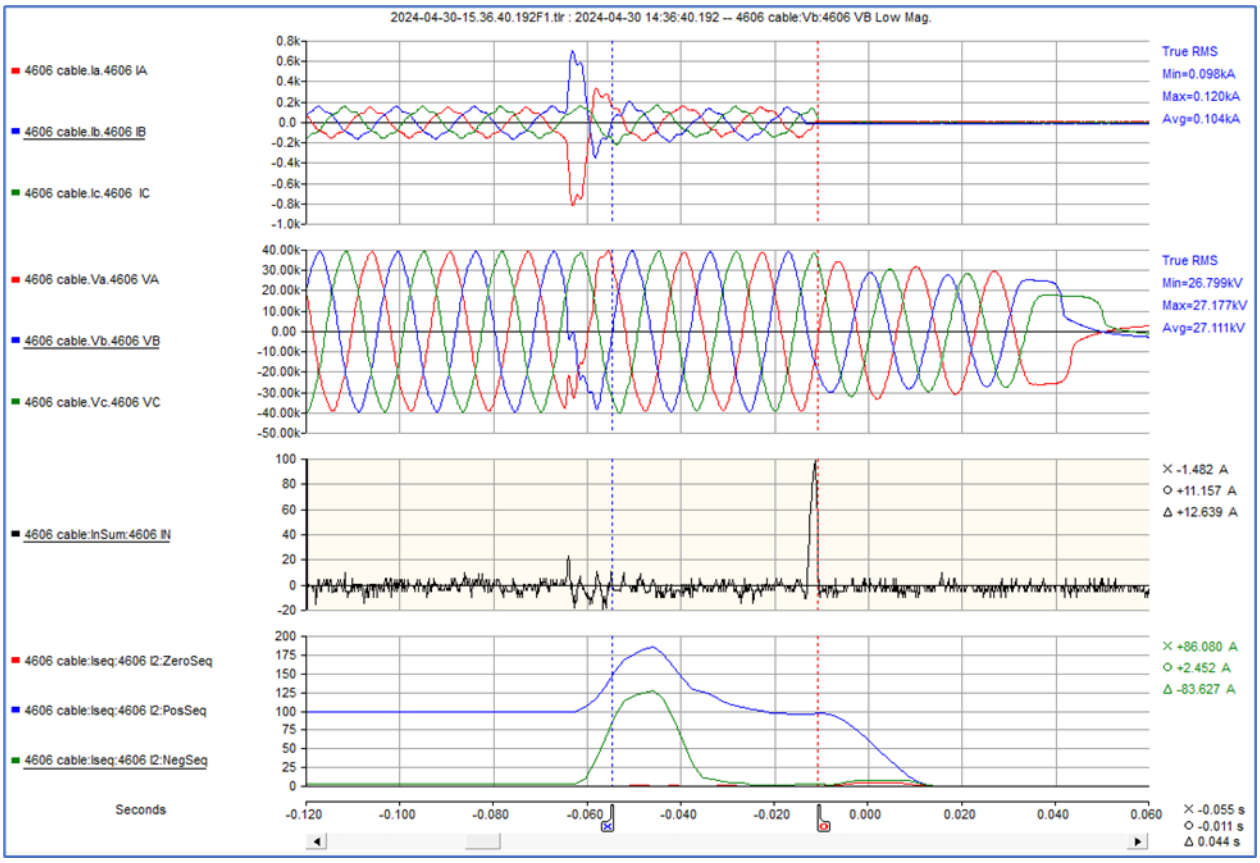

With the underground and undersea cables ruled out, that still left the L-Ave overhead 46kV bus, the L-Ave cable arrestors or VTs or the C-St 46kV GIS breaker switchgear. Close inspection and high potential testing of the L-Ave station ruled out L-Ave, leaving the C-St 46kV GIS switchgear as the last remaining culprit. A sample of gas was drawn and test and found to contain arc byproducts. The GIS switchgear was determined as being the likely source of the PD faulting event.

A detailed physical inspection of the C-St sub revealed a few issues to be addressed. For example, transformer bushings were removed and the wells inspected which uncovered rust and debris in the bushing wells. This was not a contributor to the cable event but was a further indication that some maintenance was overdue.

Summary of C-St Substation Partial Discharge (PD) Testing

Because of the level of concern over the reliability of the island power supply an external contractor was engaged to perform on-line partial discharge (PD) measurements. These were performed on May 11 and 12, 2024 on two (2) 46kV rated XLPE insulated circuits at C-St as well as L-Ave substations. The first

circuit, referred to as #1 Cable, is a submarine cable circuit which connects the L-Ave and C-St substations. The second circuit is a 46kV XLPE insulated station tie-in circuit connecting the C-St GIS system to the 46/13.2 stepdown transformer within the C-St Substation. The two cable zones tested were found to be free of partial discharge activity during normal operating voltage. However, evidence of discharge activity originating from outside the cable system was detected at the GIS at higher frequencies above 8 MHz.

These tests were repeated on September 10 and 11, 2024. The two cable zones were again found to be free of PD activity. Evidence of the PD source potentially located within the GIS was still present and was consistent with discharge activity due to foreign particles in the GIS. The test contractor advised that finding was typically not associated with imminent or medium-term concern with respect to the continued operation of the GIS. However, they did indicate that a typical remedy consisting of de-gassing, cleaning and re-gassing the GIS during a scheduled outage was advisable.

The PD activity being above 8MHz is noted to be well above the measuring range of the DFR record. The DFR having a programmed 5.76kHz sampling rate will only resolve frequencies up to 2.88kHz according to Nyquist criteria. This suggests the actual PD fault would have looked even more interesting had a higher sampling rate been used. It also suggests that the use of a higher sampling rate may resulted in the production of earlier DFR fault records even without fault triggering of the 87L relay.

Would a Wavelet Analysis of our DFR Data Offer any Improvement

While a conventional analysis of the DFR data was helpful, it was conjectured that a deeper analysis using wavelet techniques might provide better insights. As illustrated in *Figure 3*, the momentary AB phase fault self-cleared after only ½ - ¾ of a cycle. This represents an interesting and abrupt aberration to an otherwise stationary signal. For this reason, traditional 1-cycle Fourier analysis is unsuitable for this analysis. Short-time Fourier analysis may offer some improvement, but the fixed shorter window size may introduce inaccuracies because it becomes applicable to all frequencies. Therefore, this avenue was not explored. Instead, wavelet analysis was chosen to decompose the fault current signal into different frequency components.

A Short Introduction to Wavelets

The term wavelet comes from the French word ondelette meaning little wave. As the term suggests, a wavelet is a small wave of finite length, oscillatory and quickly decaying to zero. The basic concept of wavelet transform is to use a function from a wavelet family to approximate a signal. The names and shapes of four commonly used wavelet basis or mother functions [Haar, Morlet, Mexican Hat, Daubechies (dbN)] are illustrated in *Figure 4*.

Figure 4: Commonly Used Wavelet Basis/Mother Functions

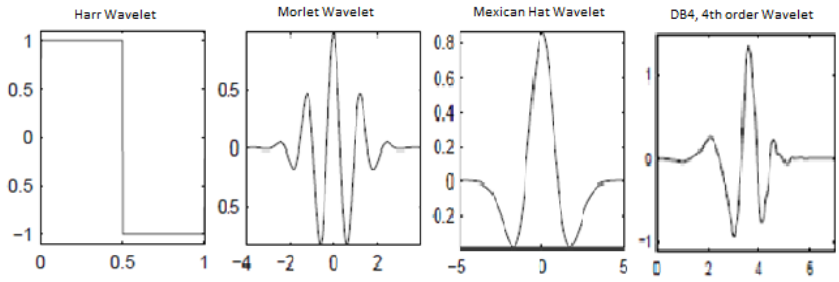

These basis functions can be described as sets of orthogonal functions (i.e., having sine and cosine terms). In a generic form, a wavelet basis function can be defined as

$$\Psi_{a,b}(t) = |a|^{-\frac{1}{2}}\Psi(\frac{t-b}{a}), a, b \in \Re, a \neq 0$$

where *a* is a scale factor that dilates or compresses a signal, reflecting the period or length of the wavelet, while *b* is a translation factor, indicating the signal's translation or position in time. In the practice, the applied wavelet function should be selected according to the specific application. The results could be very different if the different wavelet functions are selected for the same signal or time series data. The quality of the basis wavelet function is mainly determined by comparing the errors between the obtained and the theoretical result after different wavelet transforms.

The continuous wavelet transform (CWT) is the convolution of a signal *f(t)* with a selected basis wavelet function $\Psi_{a,b}(t)$ and is defined as follows:

$$CWT_f(a,b) = |a|^{-\frac{1}{2}} \int_R f(t) \cdot \Psi^*(\frac{t-b}{a})dt$$

where $\Psi_{a,b}(t)^*$ denotes the conjugate of $\Psi_{a,b}(t)$. When the scale factor $a > 1$ the signal is dilated whereas when $a < 1$ the signal is compressed. The results of the CWT are many wavelet coefficients *Cx*, which are a function of scale and position. The obtained signal data is discrete.

The discrete wavelet transform (DWT) for input signal is given as

$$DWT_f(m,n) = |{a_0}^m|^{-\frac{1}{2}} \cdot \sum_{k=1}^{N} f(k\Delta t) \cdot \Psi^*(\frac{k\Delta t - nb_0{a_0}^m}{{a_0}^m})$$

The signal function *f(t)* becomes *f(kΔt)* where the sample number *k=1,2, … , N* and *Δt* is the sampling interval. The mother wavelet is dilated and translated/shifted by selecting

$$a = {a_0}^m; b = nb_0 \cdot {a_0}^m$$

where a_0 and b_0 are fixed real positive values and where *m* and *n* are positive integers.

The signal is decomposed into sub bands with linearly increased frequency bandwidth. If scales and translations are based on a power of 2, so called dyadic transform with $a_0=2$ and $b_0=1$, the DWT will be more efficient as the algorithm uses *logarithmic* frequency coverage in contrast to the *uniform* frequency coverage of Fourier analysis.

An efficient way to implement DWT [*Ref. 1 p.1-16*] is to use a 2-channel sub-band coder scheme from Mallat tree algorithm as shown in *Figure 5*. The two output signals *A* and *D* are generated by passing the original input signal *S* through two complementary filters. *A* represents the approximation of *S* while *D* represents the details of *S*.

Figure 5: 2-channel Filter (Left) and Dyad-down Sampling (Right)

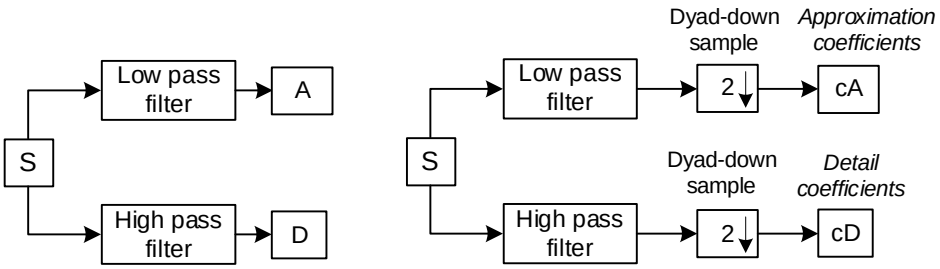

The approximation *A* is a coefficient generated by a large scaling scale, representing the low-frequency components of the signal. The detail value *D* is a coefficient generated by a small scaling scale, representing the high-frequency components of the signal. The filter coefficients are determined by the selected mother wavelet function.

Discrete wavelet transform can be represented as a tree consisting of multi-level decompositions with different low-pass and high-pass filters as shown in *Figure 6*. The decomposition process can be iterated so that the original signal is broken down into many lower resolution components. The number of levels is based on the nature of the signal and user application requirements.

Figure 6: 3-level Signal Decomposition Tree

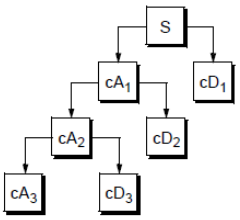

Wavelet reconstruction is the process of restoring the decomposed approximation and detail coefficients to the original signal, which is an Inverse Discrete Wavelet Transform (IDWT). In the reconstruction process, dyad-up sampling is performed, in which zeros are inserted between the samples of signal components. The signal is restored through filters from up-sampling signal components. *Figure 7* provides a block diagram description of the wavelet reconstruction process.

Figure 7: Wavelet Reconstruction

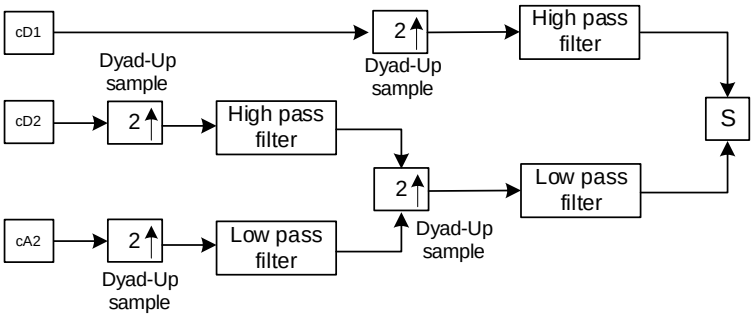

DWT and IDWT are effective tools for performing multiresolution analysis (MRA) of signals that have different frequency components occurring at different times. MRA allows for the examination of a signal with varying degrees of detail, providing good time resolution for high-frequency components and good frequency resolution for low-frequency components. Both the coarse and fine details of the signal are captured, making it possible to analyze transients and localized events effectively and present the time-frequency characteristics of the original signal.

Analysis of the DFR Record using the DWT tool Provided by a Popular EMT Application

The COMTRADE formatted DFR record of the tripping event was sampled at 5760 Hz. To perform the analysis, the COMTRADE formatted data must be read then the digitized voltage and current information restored back to one dimension of discretized data sequence. Then, the neutral current data can be processed by DWT. *Figure 8* illustrates EMT application functional blocks along with the flow of data.

Figure 8: COMTRADE File Reading and DWT Analysis

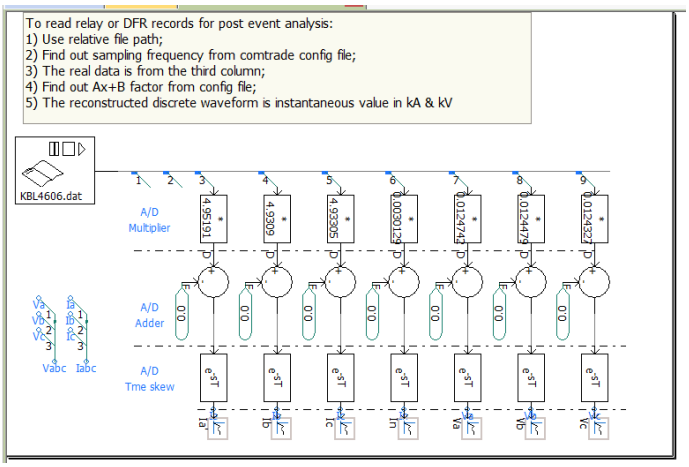

The selected mother wavelet function is 4th order Daubechies [db4] with anti-aliasing filtering enabled to maintain information fidelity. Per Nyquist criteria, the highest frequency component that can be resolved from the signal is 2.88kHz since the signal was sampled at 5.76kHz. A 5-level analysis is implemented to extract desired frequency band information and generate approximation (*A*) and detail (D) coefficients of the base signal (*S*) at each level. *Figure 9* shows frequency band information for

coefficients at each analysis level. Also refer to the block diagrams in *Figure 5* and the decomposition tree of *Figure 6*.

Figure 9: 5-Level DWT Analysis

Level	Frequency Band		Unit
	From	To	
1 - [D1]	1440	2880	Hz
2 - [D2]	720	1440	Hz
3 - [D3]	360	720	Hz
4 - [D4]	180	360	Hz
5 - [D5]	90	180	Hz
- [A5]	0	90	Hz

Approximation coefficients $A_{1\text{-}5}$ are low pass filter outputs. Think of them as the smooth part of the signal. Detail coefficients $D_{1\text{-}5}$ are high pass filter outputs. Think of them as the fine-scale or rough details, edges, and noise missing from the approximation ($A_{1\text{-}5}$) coefficients. They are the details of interest. *Figure 10* illustrates DWT decomposition of A-phase current into detail coefficients.

Figure 10: Detail (D1 to D5) Coefficients of Base Signal (S) from DWT

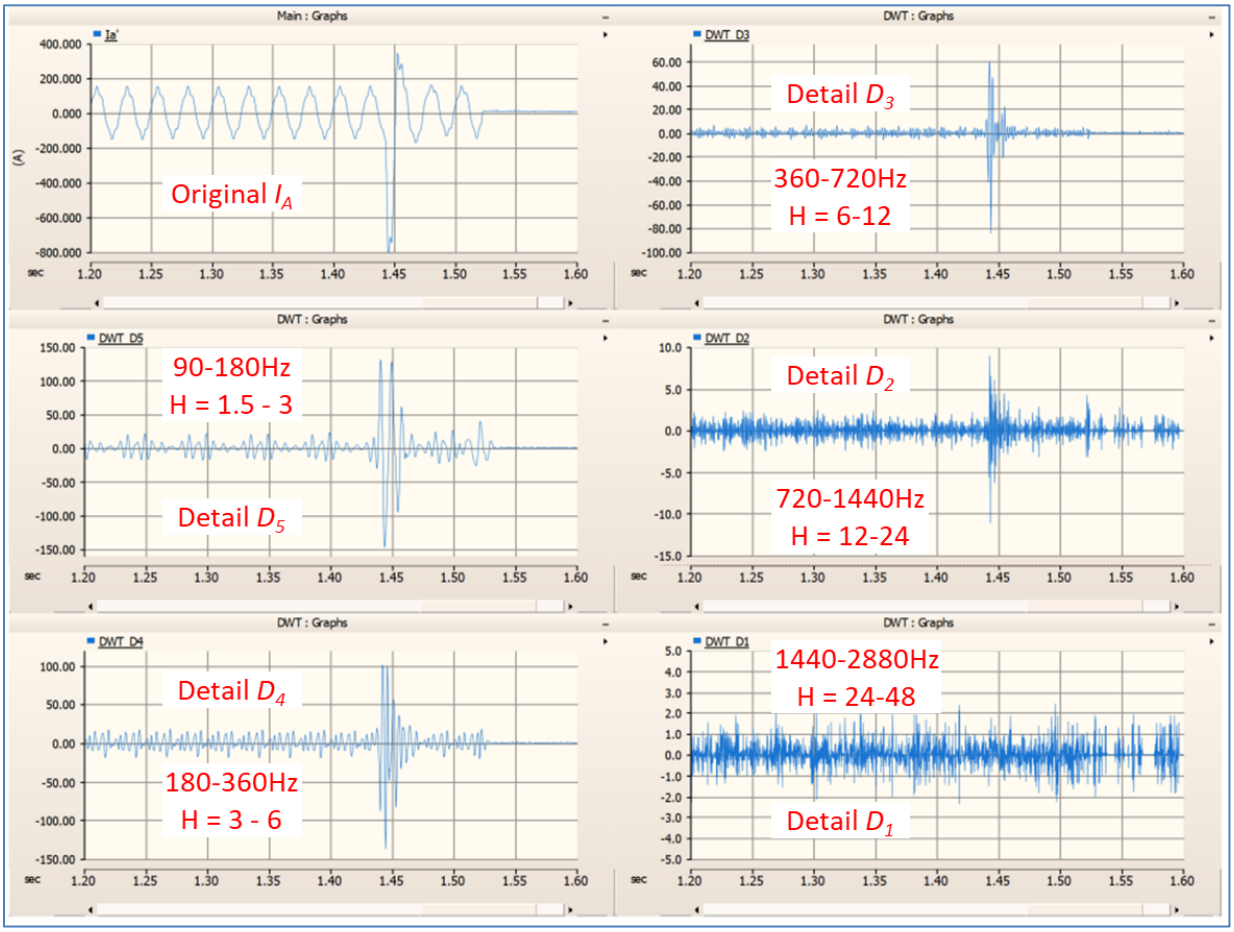

Wavelet detail coefficient D1 shows no variation of frequency components in the 1.44-2.88kHZ band (24-48th harmonic) before, during or after the fault event (occurring a little before 1.45s). Detail coefficient D2 reveals a low magnitude elevation of frequency components in 12th to 24th harmonic (720Hz-1.44kHz) range. Detail coefficient D3 shows a marked elevation of frequency components in the 6th to 12th harmonic (360-720Hz) range. Detail coefficient D4 shows a still greater elevation of frequency components in the 3rd to 6th harmonic (180-360Hz) range. Finally, detail coefficient D5 shows an even greater still elevation of frequency components in the 1.5 to 3rd harmonic (90-180Hz) range. A relatively high degree of symmetry about the horizontal (time) axis is observed indicating that the spectrum does not include much in the way of even harmonics. This is an interesting observation since the fault duration is too short for a traditional 1-cycle Fourier analysis to illustrate any symmetry about the horizontal (time) axis.

The approximation coefficient A5 shows a brief duration roughly doubling of the fundamental frequency component (60-90Hz) at the fault incident. This is consistent with tripping of the 87L relay, which would be responsive to just the fundamental frequency.

It is conjectured that the overall presence of odd harmonics is consistent with arcing behavior and the low magnitude of the original current signal consistent with a high fault impedance. All of this is consistent with PD activity though the analysis doesn't provide the confidence needed to make that a firm assumption or conclusion. Still, the DWT analysis provides a method to examine the fault signal in greater detail than was previously possible using a visual inspection or the Fourier based frequency analysis tools normally provided with DFR plotting software.

It is gratifying that the sampled gas analysis from the GIS switchgear and the follow-up PD testing was consistent with our determination of the GIS gear being the most likely location of the fault. It is possible that a higher DFR sampling rate might have yielded harmonic components beyond the 48th harmonic. While PD testing revealed PD activity above 8MHz, seeing something above the 48th harmonic might still be a certain indicator of PD activity.

Conclusions and Lessons Learned

- DWT analysis did not provide a definitive PD conclusion. However, it gave us greater detail than was available with Fourier analysis tools. It allowed us to differentiate harmonics due to load from harmonics at the fault. That makes DWT analysis a study method worth continuing.
- Recommended that higher end DFRs (more storage and higher sampling rate) be considered for installation at all three substations of interest. The higher sampling rates available may prove beneficial to improving analysis and the criticality of both an undersea cable and GIS switchgear provide suitable justification.
- It may also be suitable to replace older numerical 87L relays with those capable of travelling wave fault location. PD activity may produce travelling waves detectable by these relays if not for tripping, then at least for recording and maybe alarming.

References

1. Michel Misiti, Yves Misiti, Georges Oppenheim, Jean-Michel Poggi, *Wavelet Toolbox for Use with MATLAB: User's Guide*, Version 1, The MathWorks, Inc., March 1996.
2. Manitoba Hydro International, Ltd., *PSCAD V5 Application Help, Discrete Wavelet Transform (DWT)*, March 28, 2023.
3. Robi Polikar, *The Wavelet Tutorial: The Engineer's Ultimate Guide to Wavelet Analysis*, Rowan University, https://users.rowan.edu/~polikar/WTtutorial.html.
4. Peter Barrett Bryan, *Wavelet Convolution: Basic Principle*, Medium.com, May 25, 2022, https://peterbbryan.medium.com/wavelet-convolution-basic-principle-52fc3d71c4e6.
5. Song Ji, Irene Lu, Cory Carlson, Dean Sorensen, *Using Discrete Wavelet Transform technique to investigate high impedance fault and protection application strategy at National Grid*, Georgia Tech Protective Relaying Conference, May 2025.

Authors:

Dean Sorensen received a B.S. degree with distinction in Electrical Engineering in 1984 and an M.S. degree in Power Systems Management in 2002 both from Worcester Polytechnic Institute (WPI). He is a member of IEEE and a registered professional engineer in the state of Massachusetts. Dean has over 40 years of experience in the power industry serving in various engineering capacities in transmission, distribution, and generation primarily in the areas of protection and controls, instrumentation, and power quality. Dean is a Principal Engineer in National Grid's New England Protection Policy and Support Group and has also been a Worcester Polytechnic Institute (WPI) adjunct faculty member since 2011 teaching graduate courses and industry training classes related to power system protection.

Song Ji has been with the Department of Protection Policy and Support of National Grid since 2009. Song has 30 years' experience in the power industry.

Dan Benoit received a B.S. degree in Electrical Engineering in 2015 from University of Massachusetts: Dartmouth. He is currently a Senior Protection Engineer for National Grid's New England Protection Engineering Group. He designs, implements and maintains the protective systems for the transmission and distribution networks.